Open Access

Catalysis Research

Review

Recent Advances in the Application of Perovskite Catalysts in the Dry Reforming of Methane

Shangkun Deng [1], Yini Lei [1], Yiyu Deng [1], Yilan Lai [1], Xingyuan Gao [1, 2, *]

1. Department of Chemistry and Material Science, Guangdong University of Education, Guangzhou 510303, China; E-Mails: dengshankun@gdei.edu.cn; leiyini@gdei.edu.cn; dengyiyu@gdei.edu.cn; 2581045285@qq.com; gaoxingyuan@gdei.edu.cn
2. Engineering Technology Development Center of Advanced Materials and Energy Saving and Emission Reduction in Guangdong Colleges and Universities, Guangzhou 510303, China

* **Correspondence:** Xingyuan Gao; E-Mail: gaoxingyuan@gdei.edu.cn

Academic Editors: Wei Wang, Simone Mascotto and Bin Lin

Special Issue: Design and Development of Perovskite Materials for Energy Conversion Devices

Catalysis Research
2022, volume 2, issue 2
doi:10.21926/cr.2202012

Received: January 29, 2022
Accepted: April 20, 2022
Published: April 26, 2022

Abstract

The use of the dry reforming of methane (DRM) to convert the two principal greenhouse gases, methane and carbon dioxide, to syngas (a mixture of H_2 and CO) has attracted increasing attention in recent years. However, the DRM reaction suffers from the twin disadvantages of carbon deposition and sintering, so a highly efficient and robust catalyst with superior anti-deactivation properties is required. One way to meet this need is to incorporate active metals into crystalline oxides, such as perovskite. In this paper, recent advances in the application of perovskite catalysts in DRM are summarized, with particular attention paid to enhancing interfacial interaction, oxygen vacancies, and surface basicity. The structure-performance relationship is also discussed in depth.

Keywords

Dry reforming of methane; alloy; support; interface; oxygen vacancy; basicity

1. Introduction

Emissions of greenhouse gases arising from the rising use of fossil fuels have caused, and continue to cause, serious damage to natural ecosystems, such as rising sea levels, drought, and increasingly-frequent storms [1-13]. In the search for an alternative clean energy source, hydrogen has emerged as the most promising candidate due to its only by-product being H_2O, its carbon-free nature, and high energy density. At the same time, in the search for ways to recycle greenhouse gases, the dry reforming of methane (DRM) has attracted a great deal of attention as, through its use, -after a downstream reaction (e.g., water-gas shift reaction) or membrane separation, pure hydrogen can be generated [14-34]. In addition, the syngas produced during DRM (consisting of H_2 and the other DRM reaction product CO) can be used to synthesize other value-added chemicals through methanol production and the Fischer-Tropsch process [35-43].

However, due to the endothermic nature and high carbon content of dry reforming, metal sintering at a high temperature and coke formation deteriorate the performance of current DRM catalysts [44-56]. To combat these issues, high thermal stability and relatively low-cost perovskite-type oxides have been utilized as catalyst precursors or supports to enhance metal-support interaction (MSI) and tune the surface properties [57-60]. In addition, the perovskite structure can be partially replaced by other cations, generating a change in oxidation state and improving the redox properties [61]. Yadav et al. [62] synthesized $LaNi_{0.75}Ce_{0.05}Zr_{0.20}O_3/8MgO\text{-}SiO_2$ to improve DRM conversion efficiency, reduce carbon deposition and improve catalyst stability through enhanced MSI and strong basicity. In contrast, Alenazey et al. [63] prepared a $CeCo_xNi_{1-x}O_{3+\delta}$ perovskite catalyst by the sol-gel method that showed excellent catalytic performance for DRM due to the atomic-level mixing of metal ions and strong redox properties.

In this paper, we review recent developments in the use of perovskite structures in the preparation of catalysts for DRM and the study of the structure-performance relationship based on interface engineering, oxygen defects, and surface basicity.

2. Reaction Mechanism

The four key steps in the DRM reaction can be listed as:

a) Adsorption of CH_4 and CO_2.
b) Activation of the reactants.
c) Surface reactions to produce intermediates and products.
d) Desorption of products (e.g., CO, H_2, H_2O).

Eqn. 1 shows the main DRM reaction. This reaction is usually accompanied by a reversed water-gas shift reaction (Eqn. 2), realizing an H_2/CO ratio of less than 1 [64]. In contrast, carbon monoxide will undergo a disproportionation reaction (Boudouard reaction (Eqn. 3)) to produce carbon. The decomposition of methane also occurs (Eqn. 4), leading to carbon formation that clogs the active sites of the catalyst, inhibiting catalyst activity [16]. However, in the presence of rapid adsorption and activation of CO_2, carbon species might instead be gasified through the reverse Boudouard reaction to form CO. In the presence of perovskite, oxygen mobility and

surface oxygen concentration will be enhanced along with the migration of lattice oxygen, and an increase in oxygen defects and lattice distortion, thereby promoting the conversion of the carbon and CH_x species into gaseous products (Eqns. 5-9). The adsorption and activation of CO_2 is also promoted at the oxygen defects, releasing oxygen radicals to oxidize the carbon deposits and produce CO (Eqn. 10). However, excessive amounts of oxygen vacancies may consume H_2 and generate H_2O as a side product, which lowers the H_2 selectivity of the DRM reaction (Eqns. 11 and 12).

$$CO_2 + CH_4 \rightarrow 2H_2 + 2CO \quad (1)$$

$$CO_2 + H_2 \rightarrow H_2O + CO \quad (2)$$

$$2CO \rightarrow CO_2 + C \quad (3)$$

$$CH_4 \rightarrow C + 2H_2 \quad (4)$$

$$CH_4 + 2^* \rightarrow {CH_3}^* + H^* \quad (5)$$

$${CH_3}^* + {}^* \rightarrow {CH_2}^* + H^* \quad (6)$$

$${CH_2}^* + {}^* \rightarrow CH^* + H^* \quad (7)$$

$$CH^* + {}^* \rightarrow C^* + H^* \quad (8)$$

$$C^* + O_x \rightarrow CO + O_{x-1} + {}^* \quad (9)$$

$$CO_2 + O_{x-1} \rightarrow O_x + CO \quad (10)$$

$$4H^* \rightarrow 2H_2 + 4^* \quad (11)$$

$$H_2 + O_x \rightarrow O_{x-1} + H_2O \quad (12)$$

3. Interface Engineering

Due to carbon deposition and metal sintering, metal catalysts tend to be unstable in high-temperature reactions. Enhancing the interface interaction through, for example, the formation of alloys, or the adjustment of the MSI, is a promising strategy for improving catalytic activity [65].

3.1 Alloys

Studies have shown that, when using perovskite oxides as a precursor, Ru or Fe partially replace the A&B position of the ABO_3 structure to form alloy particles. For example, when $LnFeNi(Ru)O_3$ perovskite was adopted as a catalyst precursor for DRM, the formation of Ni-Fe-Ru alloy was found to inhibit the agglomeration of Ni clusters and prevented coking, greatly improving the catalytic activity and stability [66]. While Joo et al. introduced Fe into the layered perovskite structure $PrBaMn_{1.7}Co_{0.1}Ni_{0.2}O_{5+\delta}$, resulting in many Co-Ni-Fe ternary alloy nanoparticles forming by topological exsolution. As shown in Figures 1(a) and 1(b), under the

catalysis of ternary alloys, the consumption rates of CO_2 and CH_4 were increased by around 108.7% and 84.8%, respectively, at 900 °C. While Figure 1(c) shows that PrBaMnCoNi-15-Fe maintained excellent activity and stability even after a 350-h operation at 750 °C. According to a density functional theory (DFT) calculation, the enhanced performance of the ternary alloy sample could be attributed to the d-band center upshift and the weakened bond strengths of CH_4 and CO_2 [67].

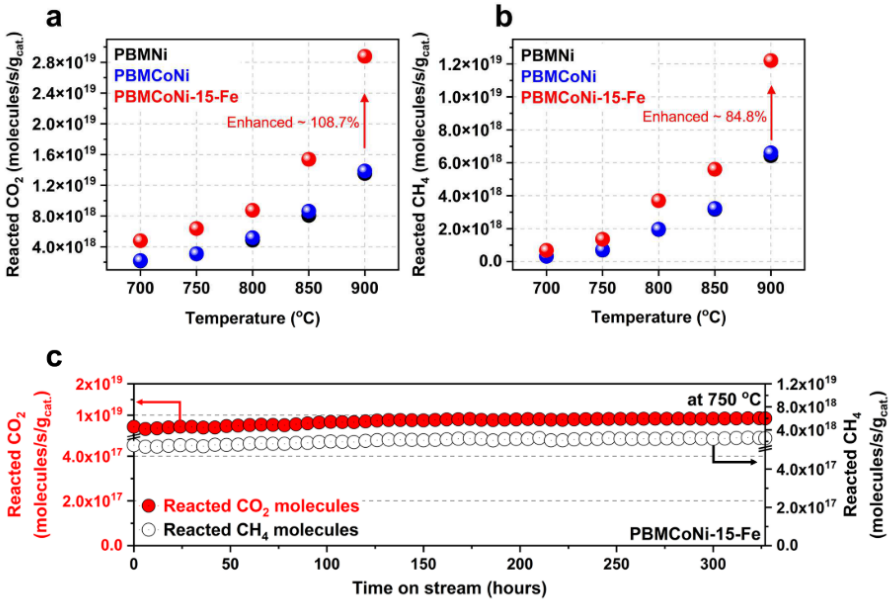

Figure 1 Catalytic properties of PrBaMnCoNi-15-Fe for the consumption of (a) CO_2 and (b) CH_4. (c) Stability test for the PrBaMnCoNi-15-Fe at 750 °C. Reproduced with permission: © 2021, Elsevier. [67].

In addition to the formation of ternary alloys, binary alloys derived from the perovskites have also been shown to benefit DRM activity. Touahra et al. [68] prepared $LaCuCoO_3$ perovskite catalysts using a citric acid-gel method and showed that after Cu partially replaced Co, the formation of a Cu-Co alloy effectively inhibited the formation of carbon, the agglomeration of active phases, and the reoxidation of CO. As well as Cu-Co alloys, Fe-Ni alloys produced from perovskites have been widely studied for DRM reactions due to their high efficiency and low cost. Shah et al. [69] manipulated the properties of -Fe-Ni alloy nanoparticles by changing the La/Fe ratio in Ni-doped $LaFeO_3$ and found that, with an optimal La/Fe ratio of 1:0.9, a larger surface area and enhanced basicity were achieved, promoting CH_4 and CO_2 adsorption and activation, while the redox properties of the Fe ions facilitated coke removal. A relatively stable conversion over 24 h operation was achieved with only 2.1 wt% carbon content. The degree of Fe-Ni synergy is determined by the Ni amount in the perovskite precursors. When $(La_{0.75}Sr_{0.25})(Cr_{0.5}Fe_{0.35}Ni_{0.15})O_3$ was used in the preparation of Fe-Ni alloys, the oxygen defects were found to be more abundant with the increasing Ni loading, which possibly resulted from the intensified reduction of Fe^{3+}/Fe^{4+}. Owing to the surface Fe-Ni alloy nanoparticles, a high methane conversion of 72% was obtained in this study, outperforming the pristine perovskite catalyst by 20 times [70]. To facilitate alloy formation, highly reducible support is favored - for example, compared with the less reducible strontium titanium ferrite (STF), which only produced a small degree of nickel--iron alloying,

lanthanum strontium ferrite (LSF) was found to be more reducible, and the alloying degree was correspondingly higher [71].

3.2 Metal-support Interaction

A strong MSI can also stabilize the active phase of a catalyst, greatly improving catalytic activity. Figueredo et al. [72] adopted nickel as the active metal and $LaAlO_3$ as the support for DRM and compared the performance of their catalysts with that of commercial α-Al_2O_3. Their results showed that the perovskite support enhanced the catalytic stability at both a high and low gas hourly space velocity (GHSV) (Figures 2(a) and 2(b)). Through the strengthened interaction between the Ni and $LaAlO_3$, the improved activity could be attributed to the generation of voids or channels between the NiO particles or supports, resulting in increased pore volume and average pore size. In addition, due to the presence of NiO, carbon nanotubes were formed on the surface of the catalyst, which enhanced metal dispersion and exposure to the reactants, thus, maintaining the catalytic stability (Figure 2(c)). Bimetallic catalysts supported on perovskite structures have also been developed. To improve the stability and activity of the catalyst, Kim et al. [73] introduced Co and Mn into a $LaNiO_3$ perovskite. They showed that the addition of Mn strengthened the Ni-La_2O_3 interaction without blocking the Ni sites. While the immediate removal of cokes by the Mn species favored CO formation between the O on the support and C on the metal surface.

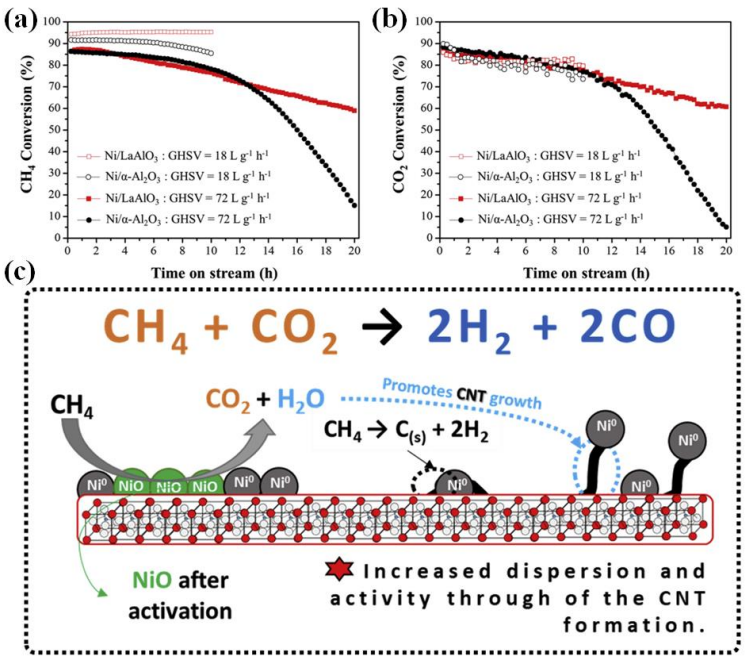

Figure 2 Stability tests in the DRM reaction in terms of the (a) H_2 and (b) CO yields with different GHSV. (c) Schematic illustration of the growth of carbon nanotubes on the surface of $Ni/LaAlO_3$. Reproduced with permission: © 2018, Elsevier. [72].

To improve dispersion, perovskite catalysts can also be supported on oxides. For example, mesoporous SiO_2 has been used as the support for $LaNiO_3$, and the dispersal of the perovskite through the SiO_2 pores did not destroy the mesoporous structure. Moreover, the migration of nickel clusters on the supported perovskite was restricted due to the strong anchoring effect,

which greatly improved the long-term catalytic stability [58, 74]. Al_2O_3 and $CeSiO_2$ have also been used as supports for perovskite catalysts [75]. In-situ XPS experiments under DRM reaction conditions showed that CO_2 oxidized the metallic nickel particles in an Al_2O_3-supported catalyst. While the use of a $CeSiO_2$ support limited the oxidation of the metal active phase. Raman spectroscopy and thermogravimetric analysis also showed that the $LaNiO_3$ supported on $CeSiO_2$ better suppressed carbon deposition than both Al_2O_3-supported $LaNiO_3$ and pristine $LaNiO_3$ (Figure 3). This was attributed mainly to the high oxygen storage capacity of $CeSiO_2$, which reacted to the presence of carbon and kept the catalyst surface free of carbon-containing residues.

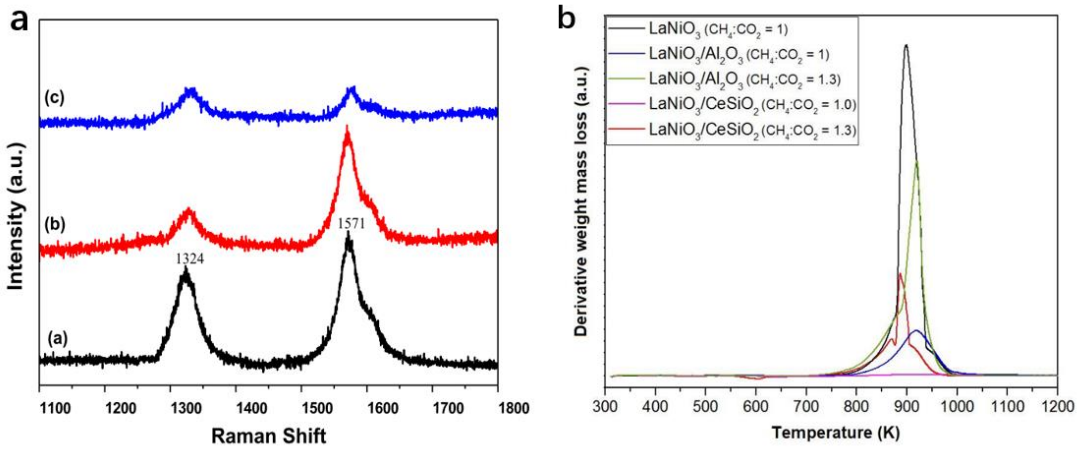

Figure 3 (a) Raman spectrum of the three catalysts after reaction (I) $LaNiO_3$ (II) $LaNiO_3/Al_2O_3$, and (III) $LaNiO_3/CeSiO_2$. (b) TPO profiles of the catalysts after a DRM reaction at 1073 K. Reproduced with permission: © 2018, Elsevier. [75].

4. Oxygen Vacancy

Oxygen vacancies promote CO_2 adsorption, accelerate the migration of oxygen atoms and enhance the anti-coking property of the host catalyst [76]. In recent studies, transition metals, rare earth metals, and alkaline earth metals have been doped into the A and B sites of perovskite catalysts to tune the concentration of oxygen vacancies [72, 77]. When alkaline earth metals were doped to the perovskite for DRM reaction, surface oxygen vacancies were seen to be produced due to the resulting valence state imbalance, facilitating CO_2 adsorption and dissociation into oxygen radicals, which gasifies the carbon species generated from the decomposition of CH_4 [78]. When $La_2Zr_{1.44}Ni_{0.56}O_{7-d}$ was partially replaced by Sr and Ca in the A site, the higher concentration of oxygen vacancy was seen to restrict the growth of Ni particles, while the mechanism of carbon reverse growth was used to explain the anti-coking ability. However, it was suggested that the shielding effect of ZrO_2 might lower the surface oxygen vacancy amount [79]. As well as alkali earth metals, the rare earth metal Ce was found to be able to partially replace at the A site of the $LaNi_{0.5}Fe_{0.5}O_3$ perovskite. The redox cycle of Ce^{3+} and Ce^{4+} rendered CeO_2 a good oxygen storage material, promoting both coke removal and high conversions in the DRM reaction [80]. In addition, transition metals have been added into perovskites to generate oxygen vacancies. Different from alkaline earth metals-doped perovskites, where lattice oxygen migration is only promoted when the perovskite structure is maintained, perovskite structures containing transition metals still possess oxygen defects and oxygen storage capacity even after the decomposition of perovskites

into pure metals and single metal oxides under the reductive and reaction conditions, facilitating CO_2 activation and carbon elimination. Shahnazi et al. synthesized $LaNiMnO_3$ (LNM) perovskite by ultrasonic spray pyrolysis, in which the substitution of Mn on the perovskite increased the specific surface area, pore size, and pore volume, leading to higher oxygen mobility, which reduced carbon deposition and transformed the carbon structure from a whisker to the amorphous type. As shown in Figure 4(a), the partial substitution of Ni by Mn enhanced the monoatomic oxygen vacancy (O^-) on the surface, which is reflected by the much higher peak intensity at 300-500 °C. As a result, the carbon deposition was greatly inhibited, as shown by the Raman spectroscopic results (Figure 4(b)). As it can be seen, the peak corresponding to ordered carbon sheets at 1583 cm^{-1} was absent with the addition of Mn; moreover, the amorphous carbon phase (the peak at around 1300 cm^{-1}) was considerably reduced due to the oxygen vacancies and mobility promoted by the redox cycle of Mn^{4+}/Mn^{3+} [81].

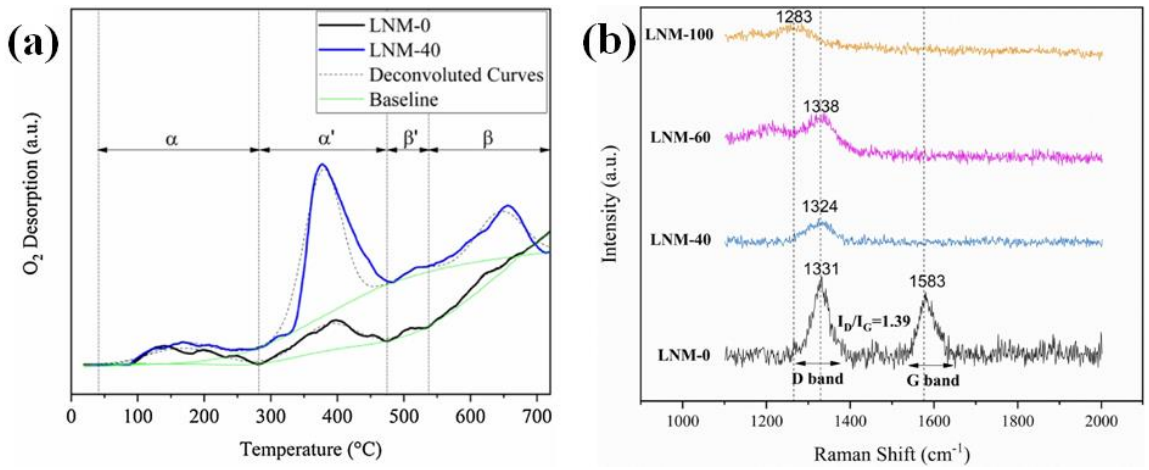

Figure 4 (a) O_2-TPD of fresh LNM, and (b) Raman spectra of the spent LNM catalysts after a 10 h DRM reaction at 750 °C. Reproduced with permission: © 2017, Elsevier. [81].

Another transition metal, Fe, has also proven effective in adjusting the number of oxygen defects in perovskite structures. Das et al. [64] developed $La_{0.9}Sr_{0.1}NiO_3$ perovskites with a partial replacement of Ni by Fe. Owing to the redox cycle between the Fe^{3+}/Fe^{4+} ions and NiFe alloys, the reversible formation and decomposition of the perovskite structure were realized, accompanied by the capture and release of oxygen, enabling a coke-resistant and stable DRM process. Similar to the case with the non-noble transition metals, $Sr_{0.92}Y_{0.08}Ti_{0.98}Ru_{0.02}O_{3+/-\delta}$ (SYTRu) was synthesized when the noble metal Ru was doped in the SYT perovskite lattice. The shift of the oxygen p-band to the Fermi level indicated a weaker Ru-O bond than the O-Ti bond, generating lower formation energy of oxygen vacancies and a higher concentration of surface oxygen, which presented a high activity in the DRM reaction [82].

5. Surface Basicity

In a perovskite catalyst, optimized basicity strengthens CO_2 adsorption [83, 84]. Ruan et al. [85] doped Si into a $LaAl_{0.25}Ni_{0.75}O_3$ perovskite to modify the structure and improve the surface basicity, facilitating CO_2 adsorption and activation, which improved the conversion efficiency and carbon

elimination. As well as the use of Si, Sr and Ni have also been added into the $LaCrO_3$ perovskite structure. The basicity was enhanced due to the presence of Sr, promoting the adsorption and dissociation of CO_2 at the basic sites during the DRM reaction [86]. Figure 5 shows the CO_2-TPD profiles of R-80, R-71, R-62 and R-53 catalysts ($La_{0.8}Cr_{0.85}Ni_{0.15}O_3$, $La_{0.7}Sr_{0.1}Cr_{0.85}Ni_{0.15}O_3$, $La_{0.6}Sr_{0.2}Cr_{0.85}Ni_{0.15}O_3$ and $La_{0.5}Sr_{0.3}Cr_{0.85}Ni_{0.15}O_3$, respectively). Two desorption peaks can be observed near 300 and 650 °C, corresponding to CO_2 desorption from the weak and strong basic sites of the catalyst. Since the amount of CO_2 desorbed was directly related to the basicity, the higher peak intensities of CO_2 desorption for R-53 indicated the promotional effect of the presence of Sr on the surface alkalinity. Sr and Ca have also been added into the $LaNi_{0.5}Fe_{0.5}O_3$ perovskite structure. Both modified perovskite catalysts exhibited a considerably larger CO_2 desorption peak than the pristine one, suggesting much stronger basicity. Due to the stronger alkalinity of Sr compared to Ca, the desorption temperature of the Sr-doped sample shifted to a higher region than the Ca-doped one, which enabled a higher conversion for the Ca-doped catalyst below 800 °C (e.g., 58.7% vs 51.5% CH_4 conversions at 750 °C).

The promotional effect of adding alkali earth metals on coke removal is the result of the basic oxide reacting with CO_2 to form carbonates or oxocarbonates, which oxidized the carbon to form a metal oxide and CO [84]. Thus, the existence of Sm_2O_3 in the $SmCoO_3$ perovskite catalyst was the origin of the improved basicity, promoting CO_2 adsorption and subsequent dissociation into oxygen radicals, which easily gasified the deposited carbon to produce CO [87]. However, in certain scenarios, the basicity may not be the dominant factor in the degree of carbon deposition. In the study of the use of $La_{0.46}Sr_{0.34}Ti_{0.9}Ni_{0.1}O_3$ in the DRM reaction, the sample was reduced at lower temperatures (700 °C) and possessed a larger number of basic sites based on the higher peak intensity of CO_2 desorption. However, surprisingly, the coke formation on the catalyst was serious following the reaction [88].

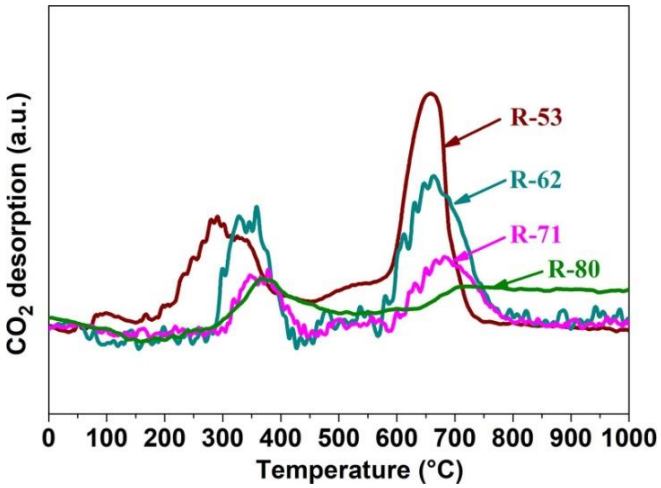

Figure 5 CO_2-TPD profiles of the reduced catalysts. Reproduced with permission: © 2020, Elsevier. [86].

6. Conclusion and Prospect

In this review, the recent progress in the application of perovskite catalysts in the DRM reaction is summarized, including the fields of interface engineering and enhancing oxygen vacancies and surface basicity. The interfacial force consists of metal-metal interactions in the alloys and the

metal-support interaction, both of which can improve the active phase dispersion. While the oxygen vacancies on the catalyst also affect the catalytic activity by accelerating the migration of oxygen atoms and improving the anti-coking ability. And the surface basicity of the catalyst is strongly related to CO_2 adsorption and activation, which enhances the conversion rate and coke removal in the DRM reaction.

Despite the progress made, there is still scope for improvement. For example, the loading of active sites derived from perovskite precursors is higher than for other precursors, which may intensify metal agglomeration and increase the cost. Advanced methods such as the impregnation of perovskite precursors onto mesoporous materials are promising solutions. Existing preparation methods for perovskites also need to be modified to satisfy industrial demand and other large-scale applications. Ball-milling is a possible solution; however, the particle size and morphology that results from the use of this approach might be a concern for the conversion efficiency in the DRM reaction.

There is also scope for the application of machine learning to the systematic search for the ideal candidate for certain reactions, as the compositional elements and the corresponding ratios can be readily incorporated into suitable models, increasing the efficiency and enabling large-scale searches. Nanocomposites combining the perovskites and other compounds (like oxides, spinels, and natural minerals) are also an attractive solution, offering several synergies. But the interface strength between each component would need to be strong. Finally, integrated reaction systems containing a catalyst (not necessarily perovskite) coated onto a gas-permeating membrane structure made of defective perovskites could enhance the conversion efficiency by driving the surface/interface mass transfer and overcoming thermodynamic limitations.

Acknowledgments

The authors gratefully thank the financial support from Guangzhou Basic and Applied Basic Research Project in China: 202102020134; Youth Innovation Talents Project of Guangdong Universities (natural science): 2019KQNCX098.

Author Contributions

S.K. Deng: Conceptualization, Data curation, Investigation, Writing - original draft, Writing - review & editing; Y.N. Lei: Conceptualization, Data curation, Investigation, Writing - original draft, Writing - review & editing; Y.Y. Deng: Data curation, Writing - original draft; Y.L. Lai: Data curation; X.Y. Gao: Funding acquisition, Resources, Project administration, Supervision, Validation.

Competing Interests

The authors have declared that no competing interests exist.

References

1. Ashok J, Ang ML, Kawi S. Enhanced activity of CO_2 methanation over Ni/CeO_2–ZrO_2 catalysts: Influence of preparation methods. Catal Today. 2017; 281: 304-311.
2. Ashok J, Pati S, Hongmanorom P, Tianxi Z, Junmei C, Kawi S. A review of recent catalyst advances in CO_2 methanation processes. Catal Today. 2020; 356: 471-489.

3. Hongmanorom P, Ashok J, Zhang G, Bian Z, Wai MH, Zeng Y, et al. Enhanced performance and selectivity of CO_2 methanation over phyllosilicate structure derived Ni–Mg/SBA–15 catalysts. Appl Catal B. 2021; 282: 119564.
4. Oh TH. Carbon capture and storage potential in coal-fired plant in Malaysia–a review. Renew Sust Energ Rev. 2010; 14: 2697-2709.
5. Chen T, Wang Z, Liu L, Pati S, Wai MH, Kawi S. Coupling CO_2 separation with catalytic reverse water–gas shift reaction via ceramic-carbonate dual-phase membrane reactor. Chem Eng J. 2000; 379: 122182.
6. Liu L, Das S, Chen T, Dewangan N, Ashok J, Xi S, et al. Low temperature catalytic reverse water–gas shift reaction over perovskite catalysts in DBD plasma. Appl Catal B. 2020; 265: 118573.
7. Yu Y, Chan YM, Bian Z, Song F, Wang J, Zhong Q, et al. Enhanced performance and selectivity of CO_2 methanation over g-C_3N_4 assisted synthesis of $NiCeO_2$ catalyst: Kinetics and DRIFTS studies. Int J Hydrog Energy. 2018; 43: 15191-15204.
8. Yu Y, Bian Z, Song F, Wang J, Zhong Q, Kawi S. Influence of calcination temperature on activity and selectivity of Ni–CeO_2 and Ni–$Ce_{0.8}Zr_{0.2}O_2$ catalysts for CO_2 methanation. Top Catal. 2018; 61: 1514-1527.
9. Bian Z, Chan YM, Yu Y, Kawi S. Morphology dependence of catalytic properties of Ni/CeO_2 for CO_2 methanation: A kinetic and mechanism study. Catal Today. 2020; 347: 31-38.
10. Gao X, Liang J, Wu L, Wu L, Kawi S. Dielectric barrier discharge plasma-assisted catalytic CO_2 hydrogenation: Synergy of catalyst and plasma. Catalysts. 2022; 12: 66.
11. Liu L, Zhang Z, Das S, Xi S, Kawi S. $LaNiO_3$ as a precursor of Ni/La_2O_3 for reverse water–gas shift in DBD plasma: Effect of calcination temperature. Energy Convers Manag. 2020; 206: 112475.
12. Hu J, Poelman H, Marin GB, Detavernier C, Kawi S, Galvita VV. FeO controls the sintering of iron-based oxygen carriers in chemical looping CO_2 conversion. J CO_2 Util. 2020; 40: 101216.
13. Oemar U, Hidajat K, Kawi S. Pd–Ni catalyst over spherical nanostructured Y_2O_3 support for oxy-CO_2 reforming of methane: Role of surface oxygen mobility. Int J Hydrog Energy. 2015; 40: 12227-12238.
14. Bian Z, Das S, Wai MH, Hongmanorom P, Kawi S. A review on bimetallic nickel-based catalysts for CO_2 reforming of methane. ChemPhysChem. 2017; 18: 3117-3134.
15. Gao X, Tan Z, Hidajat K, Kawi S. Highly reactive Ni–Co/SiO_2 bimetallic catalyst via complexation with oleylamine/oleic acid organic pair for dry reforming of methane. Catal Today. 2017; 281: 250-258.
16. Kathiraser Y, Oemar U, Saw ET, Li Z, Kawi S. Kinetic and mechanistic aspects for CO_2 reforming of methane over Ni based catalysts. Chem Eng J. 2015; 278: 62-78.
17. Li Z, Kathiraser Y, Kawi S. Facile synthesis of high surface area yolk–shell Ni@Ni embedded SiO_2 via Ni phyllosilicate with enhanced performance for CO_2 reforming of CH_4. ChemCatChem. 2015; 7: 160-168.
18. Li Z, Mo L, Kathiraser Y, Kawi S. Yolk–satellite–shell structured Ni–Yolk@Ni@SiO_2 nanocomposite: Superb catalyst toward methane CO_2 reforming reaction. ACS Catal. 2014; 4: 1526-1536.
19. Gao XY, Ashok J, Widjaja S, Hidajat K, Kawi S. Ni/SiO_2 catalyst prepared via Ni-aliphatic amine complexation for dry reforming of methane: Effect of carbon chain number and amine concentration. Appl Catal A Gen. 2015; 503: 34-42.

20. Kawi S, Kathiraser Y, Ni J, Oemar U, Li Z, Saw ET. Progress in synthesis of highly active and stable Nickel–based catalysts for carbon dioxide reforming of methane. ChemSusChem. 2015; 8: 3556-3575.
21. Gao X, Lin Z, Li T, Huang L, Zhang J, Askari S, et al. Recent developments in dielectric barrier discharge plasma-assisted catalytic dry reforming of methane over Ni-based catalysts. Catalysts. 2021; 11: 455.
22. Gao X, Liu H, Hidajat K, Kawi S. Anti-coking Ni/SiO_2 catalyst for dry reforming of methane: Role of oleylamine/oleic acid organic pair. ChemCatChem. 2015; 7: 4188-4196.
23. Gao X, Hidajat K, Kawi S. Facile synthesis of Ni/SiO_2 catalyst by sequential hydrogen/air treatment: A superior anti-coking catalyst for dry reforming of methane. J CO_2 Util. 2016; 15: 146-153.
24. Ni J, Chen L, Lin J, Schreyer MK, Wang Z, Kawi S. High performance of Mg–La mixed oxides supported Ni catalysts for dry reforming of methane: The effect of crystal structure. Int J Hydrog Energy. 2013; 38: 13631-13642.
25. Ni J, Zhao J, Chen L, Lin J, Kawi S. Lewis acid sites stabilized nickel catalysts for dry (CO_2) reforming of methane. ChemCatChem. 2016; 8: 3732-3739.
26. Gao X, Ashok J, Kawi S. A review on roles of pretreatment atmospheres for the preparation of efficient Ni-based catalysts. Catal Today. 2021. Doi: 10.1016/j.cattod.2021.06.009.
27. Bian Z, Wang Z, Jiang B, Hongmanorom P, Zhong W, Kawi S. A review on perovskite catalysts for reforming of methane to hydrogen production. Renew Sust Energ Rev. 2020; 134: 110291.
28. Li Z, Kathiraser Y, Kawi S. Facile synthesis of Multi-Ni-Core@Ni Phyllosilicate@CeO_2 shell hollow spheres with high oxygen vacancy concentration for dry reforming of CH_4. ChemCatChem. 2018; 10: 2994-3001.
29. Gao X, Ge Z, Zhu G, Wang Z, Ashok J, Kawi S. Anti-coking and anti-sintering Ni/Al_2O_3 catalysts in the dry reforming of methane: Recent progress and prospects. Catalysts. 2021; 11: 1003.
30. Gao X, Ashok J, Kawi S. Smart designs of anti-coking and anti-sintering ni-based catalysts for dry reforming of methane: A recent review. Reactions. 2020; 1: 162-194.
31. Li Z, Kathiraser Y, Ashok J, Oemar U, Kawi S. Simultaneous tuning porosity and basicity of Nickel@Nickel-Magnesium phyllosilicate core-shell catalysts for CO_2 reforming of CH_4. Langmuir. 2014; 30: 14694-14705.
32. Das S, Jangam A, Xi S, Borgna A, Hidajat K, Kawi S. Highly dispersed Ni/silica by carbonization–calcination of a chelated precursor for coke-free dry reforming of methane. ACS Appl Energy Mater. 2020; 3: 7719-7735.
33. Hu J, Hongmanorom P, Chirawatkul P, Kawi S. Efficient integration of CO_2 capture and conversion over a Ni supported CeO_2-modified CaO microsphere at moderate temperature. Chem Eng J. 2021; 426: 130864.
34. Kathiraser Y, Wang Z, Kawi S. Oxidative CO_2 reforming of methane in $La_{0.6}Sr_{0.4}Co_{0.8}Ga_{0.2}O_{3-\delta}$ (LSCG) hollow fiber membrane reactor. Environ Sci Technol. 2013; 47: 14510-14517.
35. Alves HJ, Junior CB, Niklevicz RR, Frigo EP, Frigo MS, Coimbra-Araújo CH. Overview of hydrogen production technologies from biogas and the applications in fuel cells. Int J Hydrog Energy. 2013; 38: 5215-5225.
36. Gao X, Lin X, Xie X, Li J, Wu X, Li Y, et al. Modification strategies of heterogeneous catalysts for water-gas shift reactions. React Chem Eng. 2022; 7: 551-565.

37. Faramawy S, Zaki T, Sakr AE. Natural gas origin, composition, and processing: A review. J Nat Gas Sci Eng. 2016; 34: 34-54.
38. Wang W, Wang W, Chen S. The effects of hydrogen dilution, carbon monoxide poisoning for a Pt–Ru anode in a proton exchange membrane fuel cell. Int J Hydrog Energy. 2016; 41: 20680-20692.
39. Das S, Pérez-Ramírez J, Gong J, Dewangan N, Hidajat K, Gates BC, et al. Core–shell structured catalysts for thermocatalytic, photocatalytic, and electrocatalytic conversion of CO_2. Chem Soc Rev. 2020; 49: 2937-3004.
40. Bian Z, Zhong W, Yu Y, Wang Z, Jiang B, Kawi S. Dry reforming of methane on Ni/mesoporous-Al_2O_3 catalysts: Effect of calcination temperature. Int J Hydrog Energy. 2021; 46: 31041-31053.
41. Sutthiumporn K, Maneerung T, Kathiraser Y, Kawi S. CO_2 dry-reforming of methane over $La_{0.8}Sr_{0.2}Ni_{0.8}M_{0.2}O_3$ perovskite (M = Bi, Co, Cr, Cu, Fe): Roles of lattice oxygen on C–H activation and carbon suppression. Int J Hydrog Energy. 2012; 37: 11195-11207.
42. Yang T, Kathiraser Y, Kawi S. $La_{0.6}Sr_{0.4}Co_{0.8}Ni_{0.2}O_{3-\delta}$ hollow fiber membrane reactor: Integrated oxygen separation–CO_2 reforming of methane reaction for hydrogen production. Int J Hydrog Energy. 2013; 38: 4483-4491.
43. Li Z, Das S, Hongmanorom P, Dewangan N, Wai MH, Kawi S. Silica-based micro-and mesoporous catalysts for dry reforming of methane. Catal Sci Technol. 2018; 8: 2763-2778.
44. Dewangan N, Hui WM, Jayaprakash S, Bawah AR, Poerjoto AJ, Jie T, et al. Recent progress on layered double hydroxide (LDH) derived metal-based catalysts for CO_2 conversion to valuable chemicals. Catal Today. 2020; 356: 490-513.
45. Bian Z, Kawi S. Preparation, characterization and catalytic application of phyllosilicate: A review. Catal Today. 2020; 339: 3-23.
46. Li Z, Jiang B, Wang Z, Kawi S. High carbon resistant Ni@Ni phyllosilicate@SiO_2 core shell hollow sphere catalysts for low temperature CH_4 dry reforming. J CO_2 Util. 2018; 27: 238-246.
47. Mo L, Leong KK, Kawi S. A highly dispersed and anti-coking Ni–La_2O_3/SiO_2 catalyst for syngas production from dry carbon dioxide reforming of methane. Catal Sci Technol. 2014; 4: 2107-2114.
48. Li Z, Kawi S. Multi-Ni@Ni phyllosilicate hollow sphere for CO_2 reforming of CH_4: Influence of Ni precursors on structure, sintering, and carbon resistance. Catal Sci Technol. 2018; 8: 1915-1922.
49. Das S, Ashok J, Bian Z, Dewangan N, Wai MH, Du Y, et al. Silica–ceria sandwiched Ni core–shell catalyst for low temperature dry reforming of biogas: Coke resistance and mechanistic insights. Appl Catal B. 2018; 230: 220-236.
50. Sutthiumporn K, Kawi S. Promotional effect of alkaline earth over Ni–La_2O_3 catalyst for CO_2 reforming of CH_4: Role of surface oxygen species on H_2 production and carbon suppression. Int J Hydrog Energy. 2011; 36: 14435-14446.
51. Bian Z, Kawi S. Sandwich-like Silica@Ni@Silica multicore–shell catalyst for the low-temperature dry reforming of methane: Confinement effect against carbon formation. ChemCatChem. 2018; 10: 320-328.
52. Gao X, Li J, Zheng M, Cai S, Zhang J, Askari S, et al. Recent progress in anti-coking Ni catalysts for thermo-catalytic conversion of greenhouse gases. Process Saf Environ Prot. 2021; 156: 598-616.

53. Li Z, Wang Z, Jiang B, Kawi S. Sintering resistant Ni nanoparticles exclusively confined within SiO_2 nanotubes for CH_4 dry reforming. Catal Sci Technol. 2018; 8: 3363-3371.
54. Bian Z, Suryawinata IY, Kawi S. Highly carbon resistant multicore-shell catalyst derived from Ni–Mg phyllosilicate nanotubes@silica for dry reforming of methane. Appl Catal B. 2016; 195: 1-8.
55. Ni J, Chen L, Lin J, Kawi S. Carbon deposition on borated alumina supported nano-sized Ni catalysts for dry reforming of CH_4. Nano Energy. 2012; 1: 674-686.
56. Bian Z, Kawi S. Highly carbon-resistant Ni–Co/SiO_2 catalysts derived from phyllosilicates for dry reforming of methane. J CO_2 Util. 2017; 18: 345-352.
57. Gao X, Wang Z, Ashok J, Kawi S. A comprehensive review of anti-coking, anti-poisoning and anti-sintering catalysts for biomass tar reforming reaction. Chem Eng Sci X. 2020; 7: 100065.
58. Wang N, Yu X, Wang Y, Chu W, Liu M. A comparison study on methane dry reforming with carbon dioxide over $LaNiO_3$ perovskite catalysts supported on mesoporous SBA-15, MCM-41 and silica carrier. Catal Today. 2013; 212: 98-107.
59. Pérez-Camacho MN, Abu-Dahrieh J, Goguet A, Sun K, Rooney D. Self-cleaning perovskite type catalysts for the dry reforming of methane. Chinese J Catal. 2014; 35: 1337-1346.
60. Kwon O, Huang R, Cao T, Vohs JM, Gorte RJ. Dry reforming of methane over Ni supported on $LaMnO_3$ thin films. Catal Today. 2021; 382: 142-147.
61. Moradi GR, Khosravian F, Rahmanzadeh M. Effects of partial substitution of Ni by Cu in $LaNiO_3$ perovskite catalyst for dry methane reforming. Chinese J Catal. 2012; 33: 797-801.
62. Kumar Yadav P, Das T, Mondal P. Effect of the magnesia and alumina in the modified-supported perovskite-type catalysts for the dry reforming of methane. Fuel. 2021; 302: 121233.
63. Alenazey F, AlOtaibi B, Otaibi RA, Alyousef Y, Alqahtania S, Qazaq A, et al. A Novel carbon-resistant perovskite catalyst for hydrogen production using methane dry reforming. Top Catal. 2021; 64: 348-356.
64. Das S, Bhattar S, Liu L, Wang Z, Xi S, Spivey JJ, et al. Effect of partial Fe substitution in $La_{0.9}Sr_{0.1}NiO_3$ perovskite-derived catalysts on the reaction mechanism of methane dry reforming. ACS Catal. 2020; 10: 12466-12486.
65. Carrillo AJ, Serra JM. Exploring the stability of Fe–Ni alloy nanoparticles exsolved from double-layered perovskites for dry reforming of methane. Catalysts. 2021; 116: 741.
66. Pavlova S, Kapokova L, Bunina R, Alikina G, Sazonova N, Krieger T, et al. Syngas production by CO_2 reforming of methane using $LnFeNi(Ru)O_3$ perovskites as precursors of robust catalysts. Catal Sci Technol. 2012; 210: 2099-2108.
67. Joo S, Kim K, Kwon O, Oh J, Kim HJ, Zhang L, et al. Enhancing Thermocatalytic activities by upshifting the d-Band center of exsolved Co-Ni-Fe ternary alloy nanoparticles for the dry reforming of methane. Angew Chem Int Ed. 2021; 6029: 15912-15919.
68. Touahra F, Chebout R, Lerari D, Halliche D, Bachari K. Role of the nanoparticles of Cu–Co alloy derived from perovskite in dry reforming of methane. Energy. 2019; 171: 465-474.
69. Shah S, Sayono S, Ynzunza J, Pan R, Xu M, Pan X, et al. The effects of stoichiometry on the properties of exsolved Ni–Fe alloy nanoparticles for dry methane reforming. AIChE J. 2020; 66: e17078.

70. Papargyriou D, Miller DN, Sirr Irvine JT. Exsolution of Fe–Ni alloy nanoparticles from (La,Sr)(Cr,Fe,Ni)O_3 perovskites as potential oxygen transport membrane catalysts for methane reforming. J Mater Chem A. 2019; 726: 15812-15822.
71. Thalinger R, Gocyla M, Heggen M, Dunin-Borkowski R, Grünbacher M, Stöger-Pollach M, et al. Ni–perovskite interaction and its structural and catalytic consequences in methane steam reforming and methanation reactions. J Catal. 2016; 337: 26-35.
72. Figueredo GP, Medeiros RL, Macedo HP, de Oliveira AA, Braga RM, Mercury JM, et al. A comparative study of dry reforming of methane over nickel catalysts supported on perovskite-type $LaAlO_3$ and commercial α-Al_2O_3. Int J Hydrog Energy. 2018; 43: 11022-11037.
73. Kim WY, Jang JS, Ra EC, Kim KY, Kim EH, Lee JS. Reduced perovskite $LaNiO_3$ catalysts modified with Co and Mn for low coke formation in dry reforming of methane. Appl Catal A Gen. 2019; 575: 198-203.
74. Yadav PK, Das T. Study of the perovskite-type catalysts 40$LaNi_{0.75}Fe_{0.25-X}$ M_XO_3/SiO_2 (M = Ce, Zr) for the dry reforming of methane. React Kinet Mech Catal. 2021; 1321: 279-300.
75. Rabelo-Neto RC, Sales HB, Inocêncio CV, Varga E, Oszko A, Erdohelyi A, et al. CO_2 reforming of methane over supported $LaNiO_3$ perovskite-type oxides. Appl Catal B. 2018; 221: 349-361.
76. Gonzalez-Castano M, de Miguel JN, Penkova A, Centeno MA, Odriozola JA, Arellano-Garcia H. Ni/$YMnO_3$ perovskite catalyst for CO_2 methanation. Appl Mater Today. 2021; 23: 101055.
77. Polo-Garzon F, Fung V, Liu X, Hood ZD, Bickel EE, Bai L, et al. Understanding the impact of surface reconstruction of perovskite catalysts on CH_4 activation and combustion. ACS Catal. 2018; 8: 10306-10315.
78. Dama S, Ghodke SR, Bobade R, Gurav HR, Chilukuri S. Active and durable alkaline earth metal substituted perovskite catalysts for dry reforming of methane. Appl Catal B. 2018; 224: 146-158.
79. Bhattar S, Abedin MA, Shekhawat D, Haynes DJ, Spivey JJ. The effect of La substitution by Sr- and Ca-in Ni substituted Lanthanum Zirconate pyrochlore catalysts for dry reforming of methane. Appl Catal A Genl. 2020; 602: 117721.
80. Wang M, Zhao T, Dong X, Li M, Wang H. Effects of Ce substitution at the A-site of $LaNi_{0.5}Fe_{0.5}O_3$ perovskite on the enhanced catalytic activity for dry reforming of methane. Appl Catal B. 2018; 224: 214-221.
81. Shahnazi A, Firoozi S. Improving the catalytic performance of $LaNiO_3$ perovskite by manganese substitution via ultrasonic spray pyrolysis for dry reforming of methane. J CO_2 Util. 2021; 45: 101455.
82. Kim HS, Jeon Y, Kim JH, Jang GY, Yoon SP, Yun JW. Characteristics of $Sr_{1-x}Y_xTi_{1-y}Ru_yO_{3+/-\delta}$ and Ru-impregnated $Sr_{1-x}Y_xTiO_{3+/-\delta}$ perovskite catalysts as SOFC anode for methane dry reforming. Appl Surf Sci. 2020; 510: 145450.
83. Khalesi A, Arandiyan HR, Parvari M. Effects of lanthanum substitution by strontium and calcium in La–Ni–Al perovskite oxides in dry reforming of methane. Chinese J Catal. 2008; 2910: 960-968.
84. Yang EH, Noh YS, Ramesh S, Lim SS, Moon DJ. The effect of promoters in $La_{0.9}M_{0.1}Ni_{0.5}Fe_{0.5}O_3$ (M = Sr, Ca) perovskite catalysts on dry reforming of methane. Fuel Process Technol. 2015; 134: 404-413.

85. Ruan Y, Zhao Y, Lu Y, Guo D, Zhao Y, Wang S, et al. Mesoporous $LaAl_{0.25}Ni_{0.75}O_3$ perovskite catalyst using SBA-15 as templating agent for methane dry reforming. Microporous Mesoporous Mater. 2020; 303: 110278.
86. Wei T, Jia L, Luo JL, Chi B, Pu J, Li J. CO_2 dry reforming of CH_4 with Sr and Ni co-doped $LaCrO_3$ perovskite catalysts. Appl Surf Sci. 2020; 506: 144699.
87. Osazuwa OU, Cheng CK. Catalytic conversion of methane and carbon dioxide (greenhouse gases) into syngas over samarium-cobalt-trioxides perovskite catalyst. J Clean Prod. 2017; 148: 202-211.
88. Chai Y, Fu Y, Feng H, Kong W, Yuan C, Pan B, et al. A Nickel-based perovskite catalyst with a bimodal size distribution of nickel particles for dry reforming of methane. ChemCatChem. 2018; 109: 2078-2086.